

Three-Dimensional Unsteady Euler Equations Solution on Dynamic Grids

Dave M. Belk*

Air Force Armament Laboratory, Eglin Air Force Base, Florida

J. Mark Janus,† and David L. Whitfield‡

Mississippi State University, Mississippi State, Mississippi

Abstract

AN explicit upwind second-order accurate predictor-corrector finite-volume scheme is used to solve the unsteady three-dimensional Euler equations on a dynamic body-following grid. A method for calculating fluxes at cell faces that eliminates the upstream propagation of information in supersonic regions is presented. The unsteady Euler equations are solved for the prescribed motion of a body separating from a flat plate, and time-accurate aerodynamic forces on the body are compared with forces obtained by a quasisteady approximation.

Contents

Method

The Euler equations solution method used herein is similar to that presented by Janus.¹ It is a finite-volume, flux-vector split, second-order explicit scheme that can use local time stepping with $CFL \leq 2$ on interior cells and $CFL \leq 1$ on edge cells for steady-state computations.² A different method for determining flux vectors at cell faces is presented here. This method totally eliminates the upstream propagation of information in supersonic regions. Experience with this technique has also shown that the ringing downstream of shocks characteristic of the previous method is greatly reduced. A disadvantage of the method is that in practice it frequently requires a slightly lower CFL number for stability than the previous method.

Using time-dependent curvilinear coordinates defined by

$$\xi = \xi(x, y, z, t) \quad \zeta = \zeta(x, y, z, t)$$

$$\eta = \eta(x, y, z, t) \quad \tau = t$$

the conservation law form of the Euler equations in Cartesian coordinates may be transformed to³

$$\frac{\partial Q}{\partial \tau} + \frac{\partial F}{\partial \xi} + \frac{\partial G}{\partial \eta} + \frac{\partial H}{\partial \zeta} = 0$$

For the finite-volume discretization used here, the dependent variables are stored at cell centers, but the fluxes are re-

quired at cell faces. Therefore, some type of interpolation or extrapolation must be used to determine the fluxes. The signs of the eigenvalues at the faces should determine the direction of the extrapolation to be used, but there is still some ambiguity, since the eigenvalues themselves may be calculated in several different ways at cell faces. Whitfield and Janus² computed the eigenvalues at a face from the average of dependent variables in the two cells sharing the face. The present scheme uses a different approach. Using the ξ direction, for example, the scheme reported here calculates a set of left eigenvalues, $\lambda^l(Q^L)$, and left split fluxes, $F_l(Q^L)$, from dependent variables extrapolated from cell centers left of the face, Q^L , and it also calculates a set of right eigenvalues, $\lambda^r(Q^R)$, and right split fluxes, $F_r(Q^R)$, from dependent variables extrapolated from cell centers right of the face, Q^R . The flux at the face is then set to

$$F(Q^L, Q^R) = \sum_i \left[\frac{1}{2} (\lambda^l(Q^L) + |\lambda^l(Q^L)|) F_l(Q^L) + \frac{1}{2} (\lambda^r(Q^R) - |\lambda^r(Q^R)|) F_r(Q^R) \right]$$

Note that if a left and right eigenvalue have different signs, then the corresponding split flux component may be either summed from both sides, if the sign changes from positive to negative, or from neither side, if the sign changes from negative to positive. For computational cells in which this occurs, the difference equations are inconsistent with the partial differential equation being solved, although the scheme is still conservative. An algorithm could be devised to calculate a more rational approximation of the split flux component at faces across which an eigenvalue changes sign, but this would complicate coding and vectorization. Based on the absence of any dependent variable discontinuities in the vicinity of sonic lines, this is felt to be unnecessary.

The extrapolation of dependent variables is chosen such that the algorithm is a finite-volume version of the Warming-Beam upwind scheme.³ This predictor-corrector scheme is second-order accurate in time and space and is stable for CFL numbers less than two. Edge cells (those in the domain adjacent to a boundary) are only first-order accurate and stable for a $CFL \leq 1$.

Characteristic variable boundary conditions¹ are used on all boundaries, with the exception of the reflection plate used in the moving store calculations. On the reflection plate, reflection plane boundary conditions are used.

When time accuracy is not required (steady state), the maximum time step for each individual cell is used where $CFL \leq 2$ for interior cells and $CFL \leq 1$ for edge cells. This is done to accelerate convergence by enabling every cell to advance in time as fast as possible. In situations where a time-accurate solution is desired, the minimum of all the local time steps is selected for use in all cells. This enables the

Presented as Paper 85-1704 at the AIAA 18th Fluid Dynamics, Plasmadynamics and Lasers Conference, Cincinnati, OH, July 16-18, 1985; received Jan. 20, 1986; synoptic received Jan. 30, 1987. This paper is declared a work of the U.S. Government and is not subject to copyright protection in the United States. Full paper available from AIAA Library, 555 W. 57th St., New York, NY 10019. Price: microfiche, \$4.00; hard copy, \$9.00. **Remittance must accompany order.**

*Research Scientist, Aerodynamics Branch. Senior Member AIAA.

†Graduate Student, Aerospace Department. Member AIAA.

‡Professor, Aerospace Department. Member AIAA.

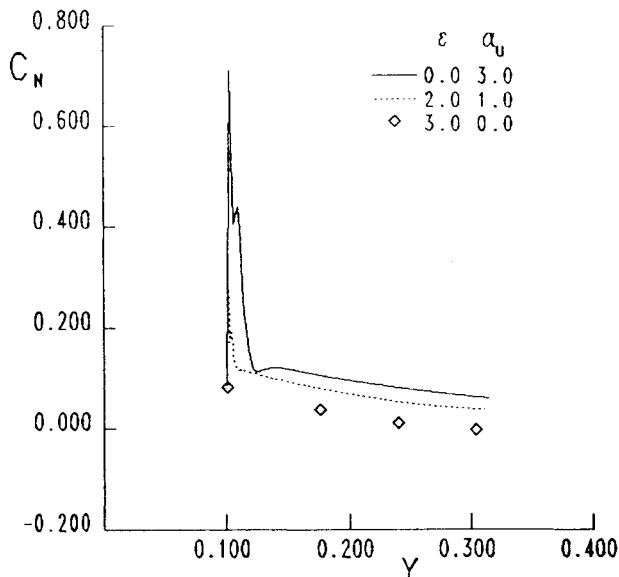


Fig. 1 Normal force coefficient vs distance from plate.

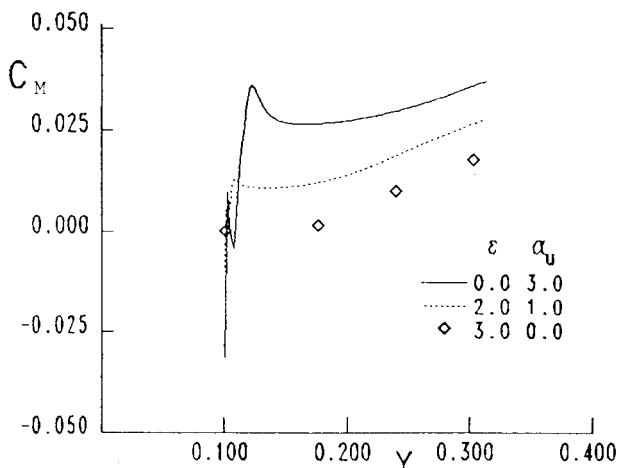


Fig. 2 Pitching moment coefficient about point at 59.8% of body length.

solution to advance to the same time level in all cells, although restricting the time step to that of the slowest cell. This method of selecting the time step is referred to as minimum time stepping. The maximum CFL for time-accurate calculations is usually restricted to 1 because of the restriction on edge cells.

Results

The case presented here is that of a 12%-thick paraboloid of revolution store launched vertically from a reflection plate. There appear to be no experimental surface pressure or flowfield data available for stores moving in the vicinity of wings or other bodies. To help assess the importance of unsteady aerodynamics during body motion such as might occur during store separation, dynamic-grid Euler solutions

were obtained from the store when launched from the vicinity of the plate in a direction perpendicular to and away from the plate. The procedure used for this calculation was to first calculate the initial steady-state flowfield with the store nose located at 10.07% of the body length away from the plate. The plunge velocity of the store away from the wall was then suddenly set to a predetermined value and held constant thereafter. Present-day store trajectory analyses typically use steady aerodynamics with a correction to the store angle of attack to account for the unsteady motion. If the freestream velocity is U_∞ and if the store has a plunge velocity of v , then the aerodynamic forces for this case are usually obtained from steady aerodynamics with the store pitch angle ϵ incremented by an amount given by $\alpha_u = \tan^{-1}(v/U_\infty)$. To evaluate the validity of this approximation, a set of steady computations were performed for a store with $\epsilon = 3$ deg and compared with two unsteady dynamic-grid computations at a Mach number of 1.41. For these calculations, a $60 \times 10 \times 15$ grid was used. The first dynamic-grid computation had $\epsilon = 0$ deg and a downward velocity such that the effective angle of attack due to the velocity α_u was 3 deg. The second dynamic-grid computation had $\epsilon = 2$ deg and an effective angle of attack increment due to the velocity α_u of 1 deg. The lower separation velocity investigated here, which is 8.08 m/s at an altitude of 3000 m, is near the upper limit for typical store separation velocities. As explained earlier, the aerodynamics for both of these unsteady cases would normally be modeled in a store separation analysis by a steady-state condition with $\epsilon = 3$ deg. A comparison of the normal force and pitching moment coefficients at various separation distances as given by unsteady calculations and by the steady-state case that models the unsteady condition is given in Figs. 1 and 2. Figure 1 shows a spike in the normal force coefficient at the first time step, which is due to apparent mass effects from the impulsive change in velocity. This is a transient effect that decays quickly. After the decay of the large transient due to store acceleration, a difference between the steady and unsteady cases still exists. This is due at least in part to the lag in the reflected shock's position for the unsteady case. The differencing in the pitching moment coefficients in Fig. 2 exhibits behavior similar to the normal force but with a much smaller initial peak.

These results illustrate the difference in aerodynamic forces for a prescribed trajectory of an unfinned store at very high separation velocities. It is possible to determine the store trajectory using forces and moments obtained from the Euler equations. To determine the significance of true unsteady aerodynamics to store separation, the rigid-body equations of motion for a finned store with a realistic initial separation velocity should be solved using both the unsteady and the steady aerodynamics so that the difference in the store trajectory can be seen.

References

- ¹Janus, J. M., "The Development of a Three-Dimensional Split Flux Vector Euler Solver with Dynamic Grid Applications," M.S. Thesis, Mississippi State Univ., Mississippi State, MS, Aug. 1984.
- ²Whitfield, D. L. and Janus, J. M., "Three-Dimensional Unsteady Euler Equations Solution Using Flux Vector Splitting," AIAA Paper 84-1552, June 1984.
- ³Warming, R. F. and Beam, R. M., "Upwind Second-Order Difference Schemes and Applications in Aerodynamic Flows," *AIAA Journal*, Vol. 14, Sept. 1976, pp. 1241-1249.